PCCP

RSC Publishing

PAPER

View Article Online
View Journal | View Issue

Cite this: *Phys. Chem. Chem. Phys.*, 2013, **15**, 18555

Optimum nanoparticles for electrocatalytic oxygen reduction: the size, shape and new design†

Guang-Feng Wei and Zhi-Pan Liu*

Received 5th September 2013,
Accepted 10th September 2013

DOI: 10.1039/c3cp53758g

www.rsc.org/pccp

The electrocatalytic oxygen reduction reaction (ORR) on nanoparticles has attracted much attention in recent years for its significance in fuel cell applications. Here by combining density functional theory (DFT) calculations with the periodic continuum solvation model based on modified-Poisson–Boltzmann (CM-MPB) electrostatics, we analyzed the ORR activity on a set of differently sized Pt nanoparticles in order to identify the optimum particles for a better designed catalyst. We show that Pt nanoparticles of ~2 nm size have the highest ORR mass activity, which is attributed to the variation of the effective reaction sites on the exposed {111} facet at the electrochemical conditions. We propose a type of a new nanocatalyst for the electrocatalytic oxygen reduction based on the knowledge from large-scale first principles simulations on Pt nanoparticles. The new catalyst has inert metal Au as the frame for the Pt nanoparticle and exposed Pt{111} sites are the active site for oxygen reduction. Such an architecture can not only prevent the initial O corrosion at the edge sites but also significantly improve the activity. The theoretical work provides a promising new direction for the rational design of a stable and active ORR catalyst *via* nano-structure engineering.

Introduction

To establish a quantitative link between the catalyst structure and its activity must rank one of the top concerns in chemistry.[1–4] Recent years have seen arising interest on nano-catalysis aiming to optimizing catalyst performance by systematically controlling the particle size and morphology. Nanostructure engineering is of practical significance for reactions catalyzed by precious metals, *e.g.* in a Pt-catalyzed electrocatalytic oxygen reduction reaction (ORR: $O_2 + 4H^+ + 4e \rightarrow 2H_2O$) since Pt is by far the best catalyst for ORR at acid conditions. To seek for better catalysts, great efforts have been devoted to fundamental research in order to identify the active site and optimum morphology of Pt nanoparticles.[5,6] Here through extensive first principles calculations on a series of Pt nanoparticles, we establish the particle size *vs.* activity trend of Pt nanoparticle from theory. To solve the poisoning problem and improve activity, we propose a general scheme to frame Pt nanoparticle using inert materials and show that such modified nanocatalysts can be three orders of magnitude more active in breaking O–O bond than unmodified particles.

For ORR on Pt nanoparticles, it remains uncertain whether activity increases or decreases with reduction in the particle size.[7–11] This is to a large extent due to the fact that nanoparticles synthesized in an experiment generally have a wide size distribution (~±2 nm), and the size and morphology can differ greatly under different experimental preparation conditions. For example, Leontyev *et al.*[12] and Shao *et al.*[13] found that in acid conditions (1 M H_2SO_4 or $HClO_4$ solution) with increase of the Pt nanoparticle size, the ORR mass activity (MA, activity per gram) first increases and then decreases: the best ORR MA was obtained at an average particle size of 2.2–2.7 nm. However, Arenz and his coworkers[7] compared the ORR activity of Pt nanoparticles of different size in 0.1 M $HClO_4$, 0.05 M H_2SO_4 and 0.1 M KOH, respectively, and found that the MA always increases with the decrease of the particle size (in a range of 1–30 nm). Nevertheless, these experimental studies indicate that the maximum variation in specific activity (activity per surface area) from polycrystalline platinum (5 mm diameter) to ultra-small Pt nanoparticles (~1 nm) is only ~5 times[7] upon the change of nanoparticle size, which implies that either the active site concentration for different particles or the activation barrier of ORR at different sites is rather constant. This picture is surprising considering that (i) the concentration of the

Shanghai Key Laboratory of Molecular Catalysis and Innovative Materials, Department of Chemistry, Key Laboratory of Computational Physical Science (Ministry of Education), Fudan University, Shanghai 200433, China. E-mail: zpliu@fudan.edu.cn

† Electronic supplementary information (ESI) available: Derivation of the realistic total surface free energy of nanoparticles, surface phase diagram of Pt nanoparticle and Au-framed Pt nanoparticles, the surface structures of IS and TSs on Pt nanoparticles under electrochemical conditions, the data of Fig.1b and our theoretical procedure for calculating the electrochemical reaction are included in the ESI. See DOI: 10.1039/c3cp53758g

surface steps/edges increases rapidly with the decrease of particle size and (ii) under ultra-high-vacuum conditions O_2 dissociation on Pt is totally dominated by stepped sites.[14]

Recent theoretical studies have shown that the oxidative species (including O and OH species) strongly poison the low coordination sites of Pt ultra-small particles ($\sim$0.5 nm) and the terrace sites have a similar problem at the reaction potentials (0.8–0.9 V).[15,16] While the stability is a major concern for the ultra-small Pt nanoparticles under acid conditions, the key issues for medium sized nanoparticles that are practically accessible (*e.g.* $>$2 nm) are to identify the active sites (*i.e.* {111}, {100} facets or on both facets) and then to design the optimum morphology and alloy composition for improving the activity, which will be the main focus of the current work.

Here by combining density functional theory (DFT) calculations with the periodic continuum solvation model based on modified-Poisson–Boltzmann (CM-MPB) electrostatics,[17] we analyzed the ORR activity on a set of differently-sized Pt nanoparticles in order to identify the optimum particles for a better designed catalyst. We rule out the role of the edges and the open {100} facets as the reaction sites of ORR in the nanoparticles due to the early surface oxygen built-up. The Pt nanoparticles of $\sim$2 nm size are predicted to have the highest ORR mass activity, which is attributed to the variation of the effective reaction sites on the exposed {111} facet at the electrochemical conditions. Our work indicates that the sharp Pt nanoparticles with maximally exposed {111} facets are higher in ORR activity and therefore the octahedron should be the optimum morphology for Pt nanoparticle. Based on the theoretical results, we propose a type of new nanocatalyst, namely, Pt nanoparticles framed by the inert metal Au, and show that this new catalyst can enhance ORR activity dramatically, suggesting a great potential for improving ORR activity *via* framed nanoparticles.

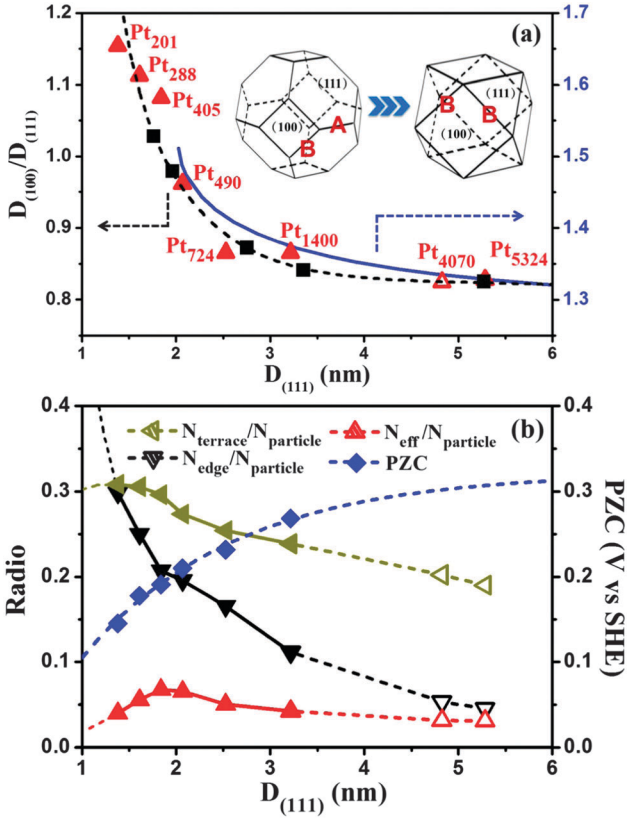

Fig. 1 (a) The size *vs.* shape ($D_{(100)}/D_{(111)}$) curves for Pt nanoparticles from experiment[12] (black) and theory (blue, also see ESI† Part I). The red points label the Pt nanoparticles utilized in this work. (b) Concentration of the surface sites of Pt nanoparticles (terrace atoms: $N_{terrace}/N_{particle}$, edge atoms: $N_{edge}/N_{particle}$ and the effective sites: $N_{eff}/N_{particle}$) and the DFT calculated potential of zero charge (PZC) value of the nanoparticles (blue points). The effective sites refer to the exposed Pt atoms at 0.9 V under electrochemical conditions.

Results and discussion

To address the nanoparticle activity, we have selected five representative Pt nanoparticles, namely, Pt_{201}, Pt_{288}, Pt_{405}, Pt_{490}, Pt_{724} and Pt_{1400}. As shown in Fig. 1a, the shape and size of these particles follows the experimentally determined shape *vs.* size curve (the red triangular points in the curve), as indicated by $D_{(111)}$ and the ratio of $D_{(100)}/D_{(111)}$ ($D_{(mkl)}$ is the average particle size along the $\langle mkl \rangle$ direction). It shows that the particle becomes sharper with the decrease of the particle size. This trend is consistent with the trend identified from theoretical calculations using DFT/CM-MPB method (see Fig. 1a blue curve) by determining quantitatively the surface free energy of all sites, including the terraces ({111} and {100}) and the edges between the terraces by minimizing the total free energy of the particle, as detailed in the ESI.† This DFT-based method was previously utilized for understanding the shape *vs.* size relationship in a photocatalytic nanoparticle TiO_2.[18]

From theory, the free energy contribution of edge sites becomes increasingly important when the particle shrinks and, as a result, the shape of very small particles deviates from Wulff thermodynamics rule that dictates the shape of a very large particle. For the Pt nanoparticles, we found that the edge sites at the {111}–{111} junction (edge-A, Fig. 1 insert) are preferred over the edge sites at {111}–{100} junction (edge-B, Fig. 1 insert). Our calculated free energy γ of the surface sites (in the absence of specific adsorption) is $\gamma_{(111)}$ = 8.32 eV nm^{-2}, $\gamma_{(100)}$ = 10.55 eV nm^{-2}, $\gamma_{(edge\text{-}A)}$ = 1.04 eV nm^{-1}, $\gamma_{(edge\text{-}B)}$ = 1.34 eV nm^{-1} (the derivation of the data can be found in the ESI,† Part I). Since the free energy of edge-A is obviously smaller than that of edge-B, the sharper shape will be energetically more favorable for the smaller particles, in which the area of {100} facet shrinks with the reduced length of edge-B. It could be mentioned that the trend of shape *vs.* size for metal nanoparticles is just opposite to that identified previously for the metal oxide (TiO_2 anatase)[18] owing to the very different nature of the edge sites (the edges of oxide particles are strongly stabilized by dissociated water).

For the Pt nanoparticles, the truncated cubes have a $D_{(100)}/D_{(111)}$value ranging from 0.58 to 0.87; the $D_{(100)}/D_{(111)}$of cuboctahedron equals 0.87, and the $D_{(100)}/D_{(111)}$ of the truncated octahedron ranges from 0.87 to 1.73 and appears only at small nanoparticles (below 2.8 nm). Interestingly, we found that both the concentration of the terrace (Fig. 1b dark green curve) and the edge Pt atoms (black curve) increase with the decrease of the particle size (down to 1 nm). This implies simply that the

ORR activity would increase down to the sub-nano scale, a highly desirable property that can be achieved by finely dispersing the nanoparticles, if (i) the nanoparticle surfaces have no poisoning adsorbates; and (ii) the barrier of ORR is constant on different nanoparticles. We therefore need to verify these two assumptions from theory.

One major complexity for studying an electrochemical process is that under electrochemical conditions (for ORR 0.8–0.9 V) the surface of the particles in contact with the aqueous solution could be covered by a finite coverage of oxidative species (O, OH, H_2O). For example, recent theoretical studies of ORR Tafel kinetics on Pt(111)[19,20] have shown that the *in situ* O coverage greatly affects the reaction equilibrium and the site blocking of the adsorbed OH plays a key role for the switch of the Tafel slope at high potentials. In this work, because of the high computational demand for large nanoparticles with adsorbates, we simplified the solid/liquid interface to be the Pt nanoparticles at various explicit O coverages and the possible H-network including H_2O or OH at the interface is taken into account by the CM-MPB model. Our previous work on Pt(111) show that this model can properly describe the ORR activity on Pt(111) since the OH merely acts as the site-blocking species during ORR.

At the steady state of ORR: the O-generation from O_2 dissociation($O_2 \rightarrow 2O$) and the O-removal towards H_2O formation ($O + 2H^+ + 2e \rightarrow H_2O$), must be in equilibrium to maintain the O-balance. The potential-dependent O coverage on nanoparticles can be determined by combining thermodynamics and the steady state kinetics analysis using DFT/CM-MPB calculations, as utilized in our previous work for characterising the *in situ* O coverage on Pt(111). In Fig. 2, we highlight the variation of the surface composition of Pt nanoparticles at the working potentials, 0.8–0.9 V *vs.* SHE and the gradual O coverage build-up with the increase of potential on a representative Pt_{221} nanoparticle is illustrated in the ESI†, Part II.

Specifically, we found that the local O coverage at the edge-sites of all Pt nanoparticles is much higher than that at the terraces over the concerned potentials (Fig. 2). In particular, each Pt at the edge-A bonds with four O atoms starting from a low potential, ~0.65 V, yielding the square planar four-coordinated PtO_4 unit (see ESI†, Part III for an enlarged view), characteristic of Pt^{4+} ion. The Pt–Pt distance for the PtO_4 unit are 3.07–3.17 Å, much longer than the 2.82–2.88 Å of Pt–Pt in the metal core. This indicates that the surface oxide initiates from the edge of Pt nanoparticles at a potential as low as 0.65 V, which is in accordance with previous theoretical calculations[21] and experiment.[22] For the open {100} facets, the O coverage is also rather high, being at least 0.5 ML at the potential higher than 0.8 V, which is similar with that found on the single crystal Pt(100) surface1.[23] For the small particles, such as Pt_{288} Pt_{405}, and Pt_{490}, the local O coverage on the {100} facets is already 1 ML even below 0.8 V. Such a high local coverage at the edge sites and the open {100} terraces prevent ORR to occur at these sites due to the low adsorption energy of O_2 molecule (<0.1 eV). The observed high O coverage at the small Pt nanoparticles can be rationalized by the enhanced electron donation ability of the small nanoparticles, as evidenced by the calculated potential of zero charge (PZC),[24] shown in Fig. 1b blue curve. It is found that the PZC of very small particles are up to 0.2 V lower compared to the large particles. For particles larger than 5 nm, it is expected that the electronic structure is already close to bulk Pt and thus the quantum size effect diminishes.

Obviously, the only likely reaction sites of ORR at the high potentials are the {111} terraces. We found that the local O coverage on {111} facets of Pt nanoparticles is generally no more than 0.5 ML: the calculated O coverage on {111} facets of Pt_{201}, Pt_{288}, Pt_{405}, Pt_{490} and P_{724} is 0.0, 0.29, 0.33, 0.14 and 0.05 ML at 0.8 V, respectively. At a high potential, the effective site, referring to those available for molecular O_2 adsorption, is reduced by up to six times as compared to the total terrace and edge sites, as shown in Fig. 1b red curve. Importantly, the effect site concentration exhibits a maximum at a particle size of ~2 nm. This is caused by the rapid O coverage built-up at small Pt nanoparticles below 2 nm, which compensates the increase of the overall surface site concentration at small particles.

To further quantify the ORR activity, we have determined the free energy barrier of O_2 direct dissociation (ΔG_a) on these Pt nanoparticles and the results are plotted in Fig. 3a. Also shown in Fig. 3c is a snapshot of the transition state (TS) of the reaction occurring on Pt_{405} nanoparticle. Our previous work shows that the TS of O–O breaking dictates the overall barrier height of ORR[20] and it is thus possible to correlate the barrier of O_2 dissociation with the ORR activity. We found that ΔG_a on all Pt nanoparticles varies in a small window, from 0.61 to 0.68 eV at high potentials (0.9 V), implying that the O_2 dissociation barrier is a local property of the Pt sites on the {111} facet, in consistence with the fact that only three Pt atoms are involved in the reaction. For ISs, the adsorbed O_2 molecule sits atop two sites and at the TSs, one O atom moves to the bridge site and the other O atom remains on the topmost site. The presence of a solvated proton ($H_7O_3^+$) nearby the top O helps to stabilize the TS and can reduce the barrier by about 0.1 eV, which is similar to that calculated on Pt(111).[20] For example, at 0.9 V, with and

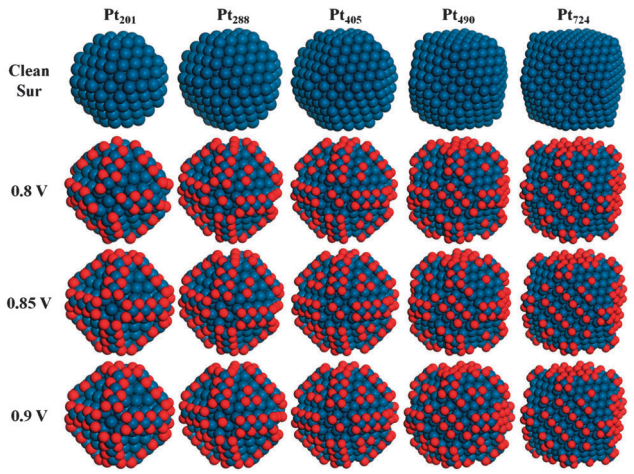

Fig. 2 Surface composition of Pt_{201}, Pt_{288}, Pt_{405}, Pt_{490} and Pt_{724} under electrochemical conditions as determined by combining thermodynamics and the steady state kinetics analysis using DFT/CM-MPB calculations. Blue ball: Pt; red ball: O.

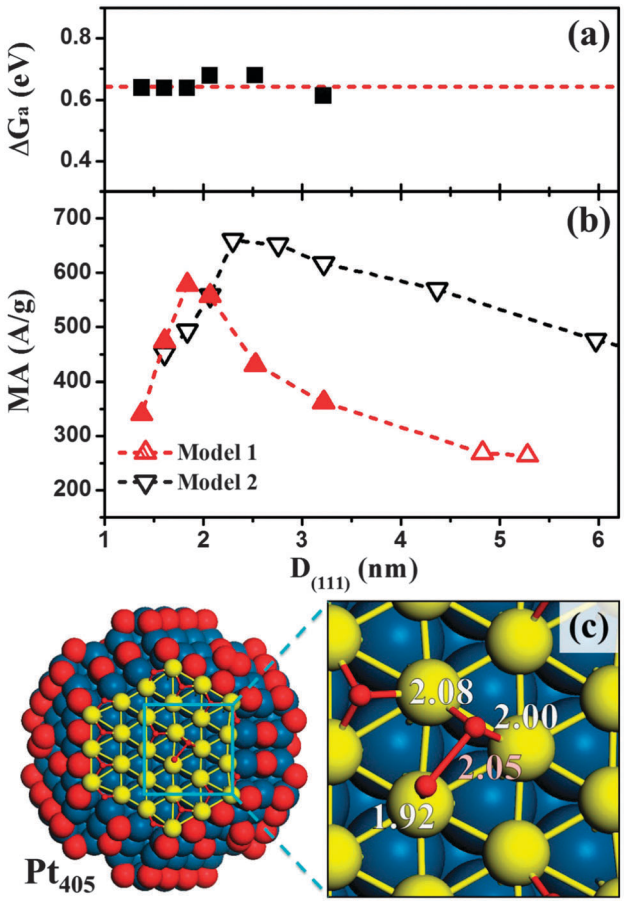

Fig. 3 Calculated ORR barrier ΔG_a (a) and MA (b) of Pt nanoparticles. The structure of TS for O_2 dissociation on a typical Pt nanoparticle is also shown in (c).

without the presence of $H_7O_3^+$ the ΔG_a on Pt_{201} is 0.64 and 0.69 eV, respectively.

It should be mentioned that our previous work of ORR Tafel kinetics on Pt(111)[20] shows that the proton-coupled O_2 dissociation ($O_2 + H_3O^+ + e \rightarrow [OOH–H_2O] \rightarrow O_{ad} + OH_{ad} + H_2O$) is a minor reaction channel at high potentials (>0.8 V) because its barrier becomes similar to that of O_2 direct dissociation at a high potential (0.8 V) and increases more rapidly with the increase of the potential. This fact appears to hold for nanoparticles: we have examined proton-coupled O_2 dissociation on Pt_{405} and the two O_2 dissociation channels have an equivalent free energy barrier at 0.78 V. Therefore, here we only utilize O_2 direct dissociation as the probe for the ORR activity over different nanoparticles.

Using the kinetics data from DFT, we can finally deduce the ORR mass activity (MA) of Pt nanoparticles. According to microkinetics, the overall current j_k of ORR can be deduced as eqn (1), where A is the pre-exponential factor ($k_{BT}/h = 6.25 \times 10^{12}$ at 300 K from classic TS theory); ΔG_a is the DFT calculated free energy barrier of the rate-determining step at 0.9 V. From Fig. 3a, we utilize a constant $\Delta G_a = 0.65$ eV in the rate calculations, which is averaged over the calculated values from five different Pt nanoparticles, considering that the nanoparticles in the experiment have a wide size distribution ($\sim\pm2$ nm) and the activity must be averaged over different size particles; θ_{O_2} is the maximum coverage of O_2 by counting the effective (111) sites on the nanoparticles. The MA of the nanoparticle can be calculated by eqn (2), where $M_{particle}$ is the mass of Pt nanoparticle.

$$j = nFS^{-1}N_A^{-1} \times A\exp(-\Delta G_a/RT)\,\theta_{O2}[H^+]\ (\mathrm{A\ cm^{-2}}) \quad (1)$$

$$\mathrm{MA} = j{\cdot}S{\cdot}N_{eff}/N_{particle}/W_{Pt}\ (\mathrm{A\ g^{-1}}) \quad (2)$$

We have calculated the MA of different Pt nanoparticles from theory (we set $p_{O2} = 1$ and $[H^+] = 0.1$) with two different models for the trend of the shape *vs.* size that determines $N_{eff}/N_{particle}$. In Model 1, the shape *vs.* size follows the experimental/theoretical trend shown in Fig. 1a. In Model 2, the shape ($D_{(100)}/D_{(111)}$) is fixed at ~1 for all sizes. We found that both models yield a similar trend for MA *vs.* size, that is, a maximum MA occurs at the nanoparticle size of ~2 nm (Fig. 3b). The calculated MA agrees generally well with those reported in the experiment. For example, the predicted MA at 2 nm particle is ~600 A g^{-1}, and the experimental value is ~500 A g^{-1}.[7] The theoretical MA also drops by ~2 times on going from a ~2 nm particle to larger particles of ~5 nm.[7,13] These indicate that the current theoretical model based on DFT/CM-MPB calculations can correctly describe the trend of activity of ORR on Pt nanoparticles.

Experimentally, one major controversy over ORR activity on nanoparticles lies in whether the specific activity (SA, the current divided by the electrochemical surface area) is independent of the particle size[6,25] or if it decreases with the decrease of the particle size,[26,27] particularly for nanoparticles below 5 nm. If the SA is independent of Pt particle size, the MA of ORR should increase on going to smaller Pt nanoparticles. On the other hand, if SA decreases with the decrease of particle size, the MA usually exhibits a peak at 2–3 nm.[28] Our theoretical results confirm the latter picture and the peak of MA from theory is ~2 nm. The observed size dependence of ORR activity can be understood from eqn (2), where the trend of the effective site concentration ($N_{eff}/M_{particle}$) determines the activity trend. Our results suggest that the MA for ORR on small Pt nanoparticles is quenched by the rapidly increased O coverage at the working potential that leads to an early surface oxidation. Therefore, we expect that the key to improve the activity of ORR on nanoparticles is to prevent the O emergence at the edge sites.

On the basis of the theoretical understanding achieved, we thus design a type of inert metal framed Pt nanoparticle catalyst, in which the inert metal (utilized here using Au atoms) replaces all the Pt atoms at edge sites, the so-called the Au-framed Pt nanoparticle. Because Au has a much lower affinity towards O atoms, one can maximally reduce the O coverage at the edges. On the other hand, the Au surfaces have lower surface energies as compared to Pt surfaces and thus the Au atoms naturally tend to accumulate at the particle surface. To further test whether the Au atoms tend to accumulate at the edge sites, we calculate the energy changes by swapping the surface Pt and Au atoms in the Au-framed Pt nanoparticle (see ESI† Part IV). We found at least 0.08 eV energy increase by simply exchanging one Pt atom with

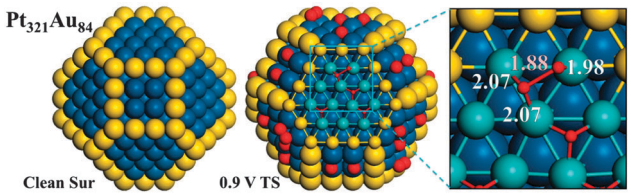

Fig. 4 Structure of a Au-framed Pt nanoparticle ($Pt_{321}Au_{84}$) and the located TS structures for O_2 dissociation at 0.9 V. The nearby solvated proton ($[H_7O_3^+]$) in solution that helps to stabilize the TS is not shown for clarity. Blue and cyan balls: Pt; yellow ball: Au; red ball: O.

the edged Au atom, which indicates that the Au-framed structure is indeed thermodynamically more stable than Pt–Au bulk alloy. Indeed, a previous work by Deng *et al.*[29] has also shown that the core–shell structure, being similar to the Au-framed particle, is thermodynamically preferred for Au–Pt nanoparticles at low Au composition.

We further evaluated the ORR activity on the Au-framed particles using DFT/CM-MPB model. In analogy to Pt_{405} and Pt_{490} of ~2 nm, two $Pt_{321}Au_{84}$ and $Pt_{394}Au_{96}$ nanoparticles were constructed. By first determining the surface phase diagram of the Au-framed Pt nanoparticles (see ESI† Part IV), we found that the apparent O coverage on $Pt_{321}Au_{84}$ and $Pt_{394}Au_{96}$ is indeed much lower than the Pt nanoparticle below 0.9 V. As shown in Fig. 4, no O adsorbs at the edge sites of $Pt_{321}Au_{84}$ at 0.8 V, in contrast to the fully O-covered edge sites on Pt_{405} at the same potential. The low O coverage on Au-framed Pt nanoparticle will enhance the stability of the nanoparticle, as measured by the surface Pt dissolution free energy[23] shown in eqn (3). Eqn (3) describes the free energy change of the dissolution/corrosion process of a surface Pt atom, corresponding to the initial step in surface corrosion.[23]

$$O_x/Au/Pt_{nanoparticle} \rightarrow O_x/Au/\square\text{–}Pt_{nanoparticle} + Pt^{2+} + 2e^- \quad (3)$$

In the process, a surface Pt ($O_x/Au/Pt_{nanoparticle}$) dissolves under the electrochemical conditions, and ends up with a surface vacancy ($O_x/Au/\square\text{–}Pt_{nanoparticle}$) on the nanoparticle. The adsorbates, such as O atoms, if present, will help to stabilize the surface vacancy. To calculate the free energy of $Pt^{2+} + 2e^-$, we have utilized the standard half-cell potential, E^0 = 1.2 V for the $Pt \rightarrow Pt^{2+} + 2e^-$ equilibrium (this means that below 1.2 V the Pt^{2+} in solution tends to adsorb and segregate as pure Pt metal at the standard conditions), as introduced in our previous work.[23] The calculated ΔG_c of $Pt_{321}Au_{84}$ is 0.20 eV higher than that of Pt_{405} at the working potential (~0.8 V), indicating the higher stability of the Au-framed nanoparticle.

Interestingly, we found that ORR can occur facilely on the Au-framed particle at the exposed Pt sites of {111} facets. The O_2 molecule can adsorb on the surface with an adsorption energy of 0.51 eV on $Pt_{321}Au_{84}$ at 0.9 V (0.75 eV at 0.75 V), which is 0.36 eV (0. 16 eV at 0.75 V) higher than it on the pure Pt particle at the same potential. Our calculated ΔG_a on $Pt_{321}Au_{84}$ and $Pt_{394}Au_{96}$ are only 0.44 and 0.37 eV, respectively, which are more than 0.20 eV lower than that on Pt_{405} (0.64 eV) and Pt_{490} (0.67 eV). From microkinetics, it can be deduced that the O_2 dissociation rate at 0.8–0.9 V (under the standard conditions) on these Au-framed particles is at least three orders of magnitude larger than that on pure Pt particles provided with the same preexpoential factor. It should be mentioned that the removal of the additional adsorbed O dissociated from molecular O_2 is facile since the adsorption energies of these additional O are all positive with respect to H_2O at the concerned potential according to the phase diagram of $Pt_{321}Au_{84}$ and $Pt_{394}Au_{96}$ (see ESI† Part IV).

To understand why the Au-framed nanoparticle can promote O_2 dissociation, we have examined the calculated TS structure for O–O dissociation on $Pt_{321}Au_{84}$ (Fig. 4), which is similar to its counterpart on Pt_{405} except that the distance of the dissociating O_2 on $Pt_{321}Au_{84}$ is much shorter (0.17 Å) than that on Pt_{405}. The shortened O–O distance at the TS implies that the Au-framed Pt nanoparticles have quite a different local electronic structure as compared to that of the pure Pt nanoparticles, which promotes O_2 activation. Considering that O_2 dissociation occurs only one lattice away from the edge sites in these 2 nm particles (*cf.* Fig. 3 and 4), it is expected that the surface-mediated poisoning due to O adsorption increases the barrier on pure Pt particles,[30] whilst the effect is absent on the Au-framed Pt nanoparticles.

We note that Yamamoto *et al.* synthesized discrete Pt-containing nanocages by using a phenylazomethine dendrimer as template for separating ultra-small Pt clusters and found that the activity of the catalyst for ORR increases with the decrease of particle size. The activity of a 0.9 nm particle is more than 10 times larger than that of 2.5 nm.[5] The essence of the confinement of Pt clusters in inert material could be the same as the Au framing strategy proposed here.

Conclusions

This work designs from theory inert metal framed Pt nanoparticles for electrocatalytic oxygen oxidation based on the atomic-level knowledge gleaned from ORR activity on pure Pt nanoparticles. We show that the active sites for ORR on Pt nanoparticles are the {111} facet at the concerned potentials (above ~0.8 V), and thus the optimum shape of Pt nanoparticles for ORR is the octahedron with maximally {111} facet exposed. The Pt nanoparticles ~2 nm are predicted to have the highest ORR mass activity since the O_2 dissociation barrier is quite similar on differently sized Pt nanoparticles and the determining factor for the activity is the effective concentration of the exposed {111} sites. By framing Pt nanoparticles using inert materials, the initial O corrosion at the edge sites can be hindered and the local activity of ORR on the PtAu surface alloy is much improved. The theoretical work provides a promising new direction for the design of a stable and active ORR catalyst *via* nano-structure engineering.

Computational methods

DFT calculations

All DFT calculations were performed using the SIESTA package[31] with numerical atomic orbital basis sets[32] and Troullier–Martins norm conserving pesudopotentials.[33] The exchange–correlation functional utilized was at the generalized gradient approximation

level, known as GGA-PBE.[34] The optimized double-ζ plus (DZP) polarization basis set with an extra diffuse function was employed for metals. The orbital-confining cutoff was determined from an energy shift of 0.010 eV. The energy cutoff for the real space grid used to represent the density was set as 150 Ry. The Quasi-Newton l-BFGS method was employed for geometry relaxation until the maximal forces on each relaxed atom were less than 0.03 eV $Å^{-1}$ and a criterion of 0.01 eV $Å^{-1}$ has been utilized to fully converge the energy of a nanoparticle larger than 2 nm. To correct the zero-point energy (ZPE), vibrational frequency calculations were performed *via* the finite-difference approach. Transition states (TSs) of the catalytic reaction were searched using our recently-developed constrained-Broyden-based TS-searching methods.[35,36]

To derive the free energy reaction profile, we first obtain the reaction energy of each step (strictly speaking, Helmholtz free energy change (ΔF) at 0 K, 0 bar) that is directly available from DFT total energy (ΔE) after the ZPE correction. For elementary surface reactions without involving the adsorption–desorption of gaseous or liquid molecules, ΔF at 0 K, 0 bar is a good approximation to the Gibbs free energy (ΔG) as the temperature T and pressure p contributions at the solid phase are small. To compute the free energy change ΔG of elementary reactions involving gaseous or liquid molecules, such as oxygen, hydrogen, and water, the large entropy term at 298 K is essential to take into account. We utilize the standard thermodynamic data[37] to obtain the temperature and pressure contributions for the G of the aqueous H_2O and gaseous H_2, which are −0.57 eV (the entropy contribution is −0.22 eV in solution) and −0.31 eV compared to the total energy of the corresponding free molecule (E, 0 K), respectively.[38] The G of O_2 is derived as $G[O_2] = 4.92$ (eV) + $2G[H_2O] - 2G[H_2]$ by utilizing OER equilibrium at the standard conditions.

Theoretical approach for studying electrochemical systems

The solid–liquid interface is modeled using the periodic continuum solvation model based on modified Poisson–Boltzmann distribution law (DFT/CM-MPB method), which has been utilized for analyzing the kinetics (Tafel curve) of an electrochemical reaction, including the Tafel lines of electro-oxidation of water to oxygen on $RuO_2(110)$,[17] first principles Tafel kinetics oxygen reduction reaction on Pt(111)[20] and Tafel kinetics for hydrogen evolution reaction on Pt and Au surfaces,[39] and also for computing the solvation contribution for solid–liquid interface reactions, such as oxygen reduction on Pt_2M skin alloys,[40] photocatalytic oxygen evolution on titania anatase[18,41] and aerobic oxidation on gold nanoparticles.[42] Here we extend this method to treating large nanoparticles. For completeness, here we briefly summarize the DFT/CM-MPB method below.

In the approach, the surface can be explicitly polarized by adding/subtracting charges and the counter charge is distributed as point charge in 3D-grid according to the modified Poisson–Boltzmann equation.[17] The absolute electrochemical potential of the system can be calculated by computing the work function in solution and then referring it to the experimental work function of the standard hydrogen electrode (SHE, 4.4–4.8 from experiment; and 4.6 V utilized in this work). The calculated potential of zero charge (pzc) of typical Pt-group metals has been benchmarked with experimental data, as shown in the ESI† Table S3, showing a good accuracy of the current approach in treating surface solvation. As also shown in the ESI† Fig. S10, our calculated differential capacitance for the initial state of O_2 activation on Pt(111) is 13 μF cm^{-2}, which is consistent with the typical experimental reported data (10–20 μF cm^{-2}).[43–46]

For a modelling reaction involving ions, for example H_3O^+, we generally also include its first solvation shell to model the reacting proton in solution, namely, $H_3O^+(H_2O)_3$ in bulk solution and $H_3O^+(H_2O)_2$ at the solid–liquid interface (the rest part of the solution is represented by the CM-MPB model). At the solid–liquid interface, two of its Hs of H_3O^+ are hydrogen-bonded with the nearby water molecules and the left H interacts with the surface electronegative species such as O_2, O and OH.

Within the DFT/CM-MPB framework, we can describe the solid–liquid interface reactions at a constant-charge mode. It is necessary to convert the kinetic data (*e.g.* barrier) obtained at the constant-charge mode to the constant-potential mode as the latter is measured in the experiment[39] (the detailed procedure for doing so has been described in our recent work on H_2 evolution on Pt and Au surfaces[36] and also briefly introduced in the ESI†). For a reaction on large nanoparticles, we found that the electrochemical potential at the TS is essentially the same as that at the IS and thus we can directly utilize the calculated electrochemical potential at the IS as the potential for the reaction to occur. For example, the difference of the computed potential at the TS and the IS is only 0.01 and 0.03 V for the O–O direct dissociation and O–OH dissociation on Pt_{288}, respectively.

Acknowledgements

We acknowledge the National Science Foundation of China (21173051, 21361130019), 973 program (2011CB808500, 2013CB834603), the Science and Technology Commission of Shanghai Municipality (08DZ2270500), the Program for a Professor of Special Appointment (Eastern Scholar) at the Shanghai Institute of Higher Learning, the China Postdoctoral Science Foundation funded project (2013M531112), and the Shanghai Postdoctoral Scientific Program (13R21410300) for financial support.

References

1 G. Ertl, *Angew. Chem., Int. Ed.*, 2008, **47**, 3524–3535.
2 G. A. Somorjai, *Surf. Sci.*, 1994, **299**, 849–866.
3 N. M. Markovic and P. N. Ross, *Surf. Sci. Rep.*, 2002, **45**, 117–229.
4 J. H. Ryu, S. S. Han, D. H. Kim, G. Henkelman and H. M. Lee, *ACS Nano*, 2011, **5**, 8515–8522.
5 K. Yamamoto, T. Imaoka, W. J. Chun, O. Enoki, H. Katoh, M. Takenaga and A. Sonoi, *Nat. Chem.*, 2009, **1**, 397–402.
6 W. C. Sheng, S. Chen, E. Vescovo and Y. Shao-Horn, *J. Electrochem. Soc.*, 2012, **159**, B96–B103.

7 M. Nesselberger, S. Ashton, J. C. Meier, I. Katsounaros, K. J. J. Mayrhofer and M. Arenz, *J. Am. Chem. Soc.*, 2011, **133**, 17428–17433.
8 F. J. Perez-Alonso, D. N. McCarthy, A. Nierhoff, P. Hernandez-Fernandez, C. Strebel, I. E. L. Stephens, J. H. Nielsen and I. Chorkendorff, *Angew. Chem., Int. Ed.*, 2012, **51**, 4641–4643.
9 K. J. J. Mayrhofer, B. B. Blizanac, M. Arenz, V. R. Stamenkovic, P. N. Ross and N. M. Markovic, *J. Phys. Chem. B*, 2005, **109**, 14433–14440.
10 J. T. Hwang and J. S. Chung, *Electrochim. Acta*, 1993, **38**, 2715–2723.
11 A. Y. Utekhina and G. B. Sergeev, *Russ. Chem. Rev.*, 2011, **80**, 219–233.
12 I. N. Leontyev, S. V. Beenov, V. E. Guterman, P. Haghi-Ashtiani, A. P. Shaganov and B. Dkhil, *J. Phys. Chem. C*, 2011, **115**, 5429–5434.
13 M. H. Shao, A. Peles and K. Shoemaker, *Nano Lett.*, 2011, **11**, 3714–3719.
14 P. Gambardella, Z. Sljivancanin, B. Hammer, M. Blanc, K. Kuhnke and K. Kern, *Phys. Rev. Lett.*, 2001, 87.
15 K. A. Persson, B. Waldwick, P. Lazic and G. Ceder, *Phys. Rev. B: Condens. Matter Mater. Phys.*, 2012, **85**, 235438.
16 L. Tang, B. Han, K. Persson, C. Friesen, T. He, K. Sieradzki and G. Ceder, *J. Am. Chem. Soc.*, 2010, **132**, 596–600.
17 Y. H. Fang and Z. P. Liu, *J. Am. Chem. Soc.*, 2010, **132**, 18214.
18 Y. F. Li and Z. P. Liu, *J. Am. Chem. Soc.*, 2011, **133**, 15743–15752.
19 A. Holewinski and S. Linic, *J. Electrochem. Soc.*, 2012, **159**, H864–H870.
20 G. F. Wei, Y. H. Fang and Z. P. Liu, *J. Phys. Chem. C*, 2012, **116**, 12696–12705.
21 J. Rossmeisl, J. K. Norskov, C. D. Taylor, M. J. Janik and M. Neurock, *J. Phys. Chem. B*, 2006, **110**, 21833–21839.
22 N. M. Markovic and P. N. Ross, *Surf. Sci. Rep.*, 2002, **45**, 121–229.
23 Y. H. Fang and Z. P. Liu, *J. Phys. Chem. C*, 2010, **114**, 4057–4062.
24 Y. H. Fang, G. F. Wei and Z. P. Liu, *Catal. Today*, 2013, **202**, 98–104.
25 H. Yano, J. Inukai, H. Uchida, M. Watanabe, P. K. Babu, T. Kobayashi, J. H. Chung, E. Oldfield and A. Wieckowski, *Phys. Chem. Chem. Phys.*, 2006, **8**, 4932–4939.
26 K. Kinoshita, *J. Electrochem. Soc.*, 1990, **137**, 845–848.
27 K. J. J. Mayrhofer, D. Strmcnik, B. B. Blizanac, V. Stamenkovic, M. Arenz and N. M. Markovic, *Electrochim. Acta*, 2008, **53**, 3181–3188.
28 G. A. Tritsaris, J. Greeley, J. Rossmeisland and J. K. Norskov, *Catal. Lett.*, 2011, **141**, 909–913.
29 L. Deng, W. Y. Hu, H. Q. Dengand and S. F. Xiao, *J. Phys. Chem. C*, 2010, **114**, 11026–11032.
30 Z. P. Liu and P. Hu, *J. Am. Chem. Soc.*, 2003, **125**, 1958–1967.
31 J. M. Soler, E. Artacho, J. D. Gale, A. Garcia, J. Junquera, P. Ordejonand and D. Sanchez-Portal, *J. Phys.: Condens. Matter*, 2002, **14**, 2745–2779.
32 J. Junquera, O. Paz, D. Sanchez-Portaland and E. Artacho, *Phys. Rev. B: Condens. Matter*, 2001, **64**, 9.
33 N. Troullierand and J. L. Martins, *Phys. Rev. B: Condens. Matter*, 1991, **43**, 1993–2006.
34 J. P. Perdew, K. Burke and M. Ernzerhof, *Phys. Rev. Lett.*, 1996, **77**, 3865–3868.
35 H. F. Wang and Z. P. Liu, *J. Am. Chem. Soc.*, 2008, **130**, 10996–11004.
36 C. Shang and Z. P. Liu, *J. Chem. Theory Comput.*, 2010, **6**, 1136–1144.
37 *CRC Handbook of Chemistry and Physics*, ed. D.R.Lide, CRC press, 2003–2004.
38 Z. P. Liu, S. J. Jenkins and D. A. King, *J. Am. Chem. Soc.*, 2004, **126**, 10746–10756.
39 Y. H. Fang, G. F. Wei and Z. P. Liu, *J. Phys. Chem. C*, 2013, **117**, 7669–7680.
40 G. F. Wei and Z. P. Liu, *Energy Environ. Sci.*, 2011, **4**, 1268–1272.
41 Y. F. Li, Z. P. Liu, L. L. Liu and W. G. Gao, *J. Am. Chem. Soc.*, 2010, **132**, 13008–13015.
42 C. Shang and Z. P. Liu, *J. Am. Chem. Soc.*, 2011, **133**, 9938–9947.
43 A. Cuesta, *Surf. Sci.*, 2004, **572**, 11–22.
44 V. Climent, G. A. Attard and J. M. Feliu, *J. Electroanal. Chem.*, 2002, **532**, 67–74.
45 T. Pajkossy and D. M. Kolb, *Electrochem. Commun.*, 2003, **5**, 283–285.
46 N. Garcia-Araez, V. Climent, E. Herrero, J. M. Feliu and J. Lipkowski, *Electrochim. Acta*, 2006, **51**, 3787–3793.